Available online at www.sciencedirect.com
SCIENCE DIRECT®
Thermochimica Acta 432 (2005) 112–123
thermochimica acta
www.elsevier.com/locate/tca

High temperature properties of by-product cold bonded pellets containing blast furnace flue dust

Ryan Robinson *

Luleå University of Technology, SE-97187 Luleå, Sweden

Received 23 November 2004; received in revised form 21 March 2005; accepted 7 April 2005

Abstract

In this investigation, the fundamental reactions occurring during the heat treatment of cold bonded pellets (CBP) comprised of iron and steelmaking by-products have been studied. Blast furnace (BF) flue dust, which contains fractions of coal and coke particles, has been included in the CBP blend as a source of solid reductant. Thermal analysis was performed on CBP samples in inert atmosphere at a heating rate of 10 °C/min in order to observe their high temperature properties, specifically, the mechanisms of self-reduction within CBPs. Both endothermic and exothermic reactions were observed during heating. The gases generated during thermal analysis were analyzed using a quadropole mass spectrometer (QMS). Furthermore, CBP samples heated to several different temperatures and quenched in argon were analyzed using X-ray diffraction (XRD) and scanning electron microscopy (SEM). Results from this investigation demonstrate that the decomposition of hydrates and carbonates in CBP samples contribute, as gaseous intermediates, to an earlier reduction of contained iron oxides. The gaseous intermediates are responsible for an initial gasification of carbon contained in blast furnace flue dust leading to low temperature iron oxide reduction. The step-wise reduction of iron oxides in CBPs at the given conditions begins at ∼500 °C and is nearly completed at 1200 °C. This work can help to provide a fundamental understanding of the reduction characteristics of iron and steelmaking by-product agglomerates.

Keywords: Cold bonded pellets (CBP); Iron oxide reduction; By-products; Thermal analysis

1. Introduction

In the global steel industry, more than 400 kg of solid by-product is generated per ton of steel produced. Most of this by-product (70–80%) is in the form of slag, which after much research, is now used largely in the cement industry and for road and civil construction. The remaining solid by-products can be classified as dusts, sludge and oily/non-oily mill scale. Traditionally, the majority of generated dust, sludge and scale are recycled back to the BF by means of the sintering process. In Sweden, all sinter plants have been closed due to environmental regulation thereby halting the consumption of these solid by-products as recycle in blast furnaces. Barring a sintering process, the fraction of solid by-products classified as fine particles (60% of dusts and sludge) is very difficult to recycle without extensive pre-treatment and until recently has been by in large deposited in landfills. These by-products are problematic to recycle not only because of their small particle size but also for their high content of impurities of which the saleable content is not high enough to make further processing economical [1,2]. In recent years, as costs for depositing solid by-products from the steel industry in landfills have increased due to lack of space and increasing environmental restrictions, the recycling of these solid by-products, not only to avoid depositing costs but also to recover valuable iron metal fractions, has become a near necessity. Hence, recycling of various by-products as cold bonded agglomerates in the BF has become a regular practice in Sweden [3].

The optimization of reduction properties of cold bonded agglomerates, containing by-product oxides from the steel industry, is essential for the beneficial recovery and use of the agglomerated iron and carbon units during recycling. While there have been earlier studies of the high temperature be-

* Tel.: +46 920 49 13 09; fax: +46 920 49 11 99.
E-mail address: ryan.robinson@ltu.se.

0040-6031/$ – see front matter © 2005 Elsevier B.V. All rights reserved.
doi:10.1016/j.tca.2005.04.015

havior of metallurgical by-product agglomerates containing a supplementary carbon source [4,5] and iron ore mixed with a supplementary carbon source [6], few studies have thoroughly investigated the high temperature properties of cold bonded by-product agglomerate mixes utilizing the carbon content in BF flue dust as a carbon source in self-reducing by-product pellets.

The objective of the present work is to describe the thermal behavior of cold bonded pellets containing BF flue dust, various other metallurgical by-products and Portland cement. Pellet samples have been tested using thermal analysis coupled with QMS gas analysis at temperatures ranging from 20 to 1250 °C in argon gas. Thermal analysis results are complemented with phase and morphological investigations.

2. Materials and methods

2.1. Cold bonded by-product pellets (CBPs)

Samples of prefabricated CBPs having a composition similar to that of cold bonded briquettes currently recycled in the BF at SSAB Tunnplåt AB in Luleå, Sweden were investigated. The pellets were produced on a lab scale basis using the following procedure: 20 kg sample that consists of by-products and cement was mixed in a drum mixer for 4 min, then the blend was emptied into a container and mixed with water (12.5–13.5 wt.%) for another 2 min. After mixing again and left standing for 20 min, the pellet mass was fed into the disc pelletizer run at a rotating speed of 18 rpm and an angle of 45°. The pellet mass was left to rotate in the pelletizer for 20 min. The green pellets were spread out onto the floor and left to cure for 1 h. Afterwards, the pellets were stored in a container for an additional 24 h before sieving. Pellets in the size fraction of 9–12.5 mm were used in this study.

The CBP blend contains basic oxygen furnace (BOF) fine and coarse sludge, BF flue dust, diverse filter dusts and cold bonded briquette fines. Contents of scrap fines, present in cold bonded briquettes currently recycled at SSAB Tunnplåt AB, were excluded from the CBP blend due to their incompatible particle size. The chemical composition of the raw materials in CBPs is given in Table 1 as well as the pellet composition and particle size in Table 2.

Table 2
Pellet composition and particle size of materials

Material	Wt.%	−100 μm fraction (%)
BOF coarse sludge	35	34.3
BOF fine sludge	20	39.3
BF flue dust	20	57.9
Briquette fines	10	12.9
Portland cement	10	100.0
Filter dust	5	100.0
Total	100	47.7

2.2. Thermal analysis

A Netzsch STA 409 instrument equipped with simultaneous thermogravimetric (TG), differential thermal analysis (DTA) coupled with a QMS was used to study the high temperature properties of CBPs. The sensitivity of this STA instrument is ±1 μg. A schematic diagram of the thermal analysis instrument is given in Fig. 1. An initial sample was prepared by crushing and grinding 50 g of CBPs to a size of −75 μm and was thoroughly mixed in order to homogenize the material for subsequent thermal analysis experiments.

Two types of tests were performed on the CBP sample. First, to determine the temperature intervals of interest, dynamic TG/DTA/QMS tests were conducted on sub-samples weighing ∼70 mg. Two alumina crucibles, one containing alumina powder as a reference and the other a CBP sample, were heated from 20 to 1200 °C at a heating rate of 10 °C/min in argon with a constant flow rate of 200 ml/min.

Second, to investigate phase and morphology structure at various temperatures, additional TG tests were conducted on sub-samples weighing between 2 and 2.5 g. A larger alumina crucible with CBP sample was used for TG experiments, exclusive of DTA and QMS analysis, with a heating program comprised of a controlled dynamic heating to various temperatures and then an isothermal heating for 1 h. The temperature versus time layout for the experiments is given in Fig. 2. The dynamic heating rates ranged from 5 to 10 °C/min and ar-

Table 1
Chemical composition of raw materials for cold bonded pellets (wt.%)

	BOF fine	BOF coarse	Filter dust	BF-1 flue	BF-2 flue	Portland cement	Briquette fines
Fe_{tot}	53.70	74.40	65.80	30.80	35.60	2.40	39.3
CaO	13.90	9.62	0.56	6.54	6.52	62.00	16.60
SiO_2	1.04	1.97	1.65	4.12	4.39	20.00	6.44
MnO	0.97	0.94	0.26	0.74	0.59	–	0.97
P_2O_5	0.07	0.14	0.05	0.04	0.05	–	0.11
Al_2O_3	0.10	0.15	0.39	1.54	1.55	4.40	1.96
MgO	3.35	3.19	1.16	1.34	1.72	3.05	3.27
K_2O	0.05	0.04	0.31	0.03	0.04	1.40	0.10
TiO_2	0.09	0.31	0.23	0.20	0.29	–	0.49
Cr_2O_3	0.06	0.08	0.19	0.03	0.05	–	0.11
C	1.64	1.01	0.55	35.3	30.6	–	11.7

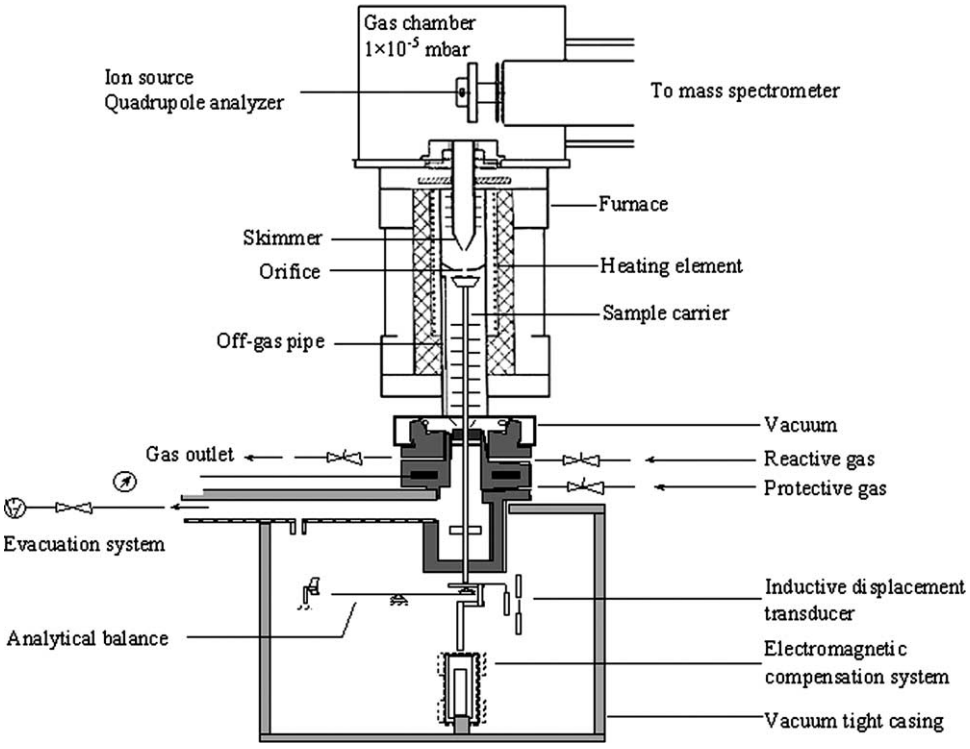

Fig. 1. Thermal analysis instrument.

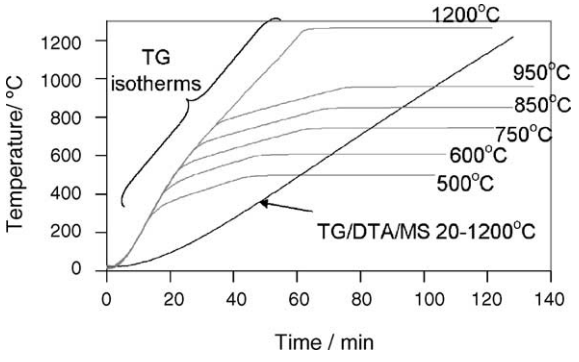

Fig. 2. Temperature vs. time for the thermal analysis experiments.

gon gas was used as in the first experiments. The precision, defined as 2σ, of TG data for all tests was ± 1.95 wt.%.

2.3. Reduction degree

Due to the relative small sample sizes used in this investigation, chemical analysis of the samples after thermal treatment was not feasible. Therefore, an attempt to calculate reduction degree was done using results from chemical analysis, TG/DTA analysis and gas analysis (intensities I_{CO} and I_{CO_2} given in Table 3) in Eqs. (1)–(3). Reduction degree has been defined as follows:

$$\mathrm{RD}\,(\%) = \left[\frac{\Delta m_{\mathrm{O,red}}}{m_{\mathrm{O,initial}}}\right] \times 100 \tag{1}$$

where RD (%) is the reduction degree, $\Delta m_{\mathrm{O,red}}$ is the change in mass due to oxygen removal from iron oxide, $m_{\mathrm{O,initial}}$ is the initial mass of oxygen bound to iron,

$$m_{\mathrm{O,initial}} = 100 - m_{\mathrm{Fe_{tot}}} - m_{\mathrm{oxides}} - m_{\mathrm{CO_2,carbonates}} - m_{\mathrm{H_2O}} \tag{2}$$

where $m_{\mathrm{Fe_{tot}}}$ is the initial wt.% of total Fe from chemical analysis, m_{oxides} is the initial wt.% of oxides other than iron oxide from chemical analysis, $m_{\mathrm{CO_2,carbonates}}$ is the initial wt.% of CO_2 from TG data in the temperature transition 680–760 °C, $m_{\mathrm{H_2O}}$ is the initial wt.% of H_2O from TG data in the temper-

Table 3
Maximum CO and CO_2 gas intensities (I) for a CBP sample at different temperature intervals

Temperature range	I_{CO}	I_{CO_2}	$I_{CO}/(I_{CO}+I_{CO_2})$	$I_{CO_2}/(I_{CO}+I_{CO_2})$
500–600 °C	1.89E − 10	3.99E − 10	0.32	0.68
600–750 °C	6.43E − 10	1.46E − 09	0.31	0.69
750–850 °C	5.94E − 10	1.10E − 09	0.35	0.65
850–950 °C	1.16E − 09	2.78E − 10	0.81	0.19
950–1200 °C	4.10E − 09	8.09E − 10	0.84	0.16
S.E.	–	–	0.01	0.01

ature transition 40–480 °C,

$$\Delta m_{\mathrm{O,red}} = \Delta m_{\mathrm{total,red}} \times \left[\frac{M_{\mathrm{O}} I_{\mathrm{CO}}}{M_{\mathrm{CO}}(I_{\mathrm{CO}} + I_{\mathrm{CO_2}})} + \frac{M_{\mathrm{O_2}} I_{\mathrm{CO_2}}}{M_{\mathrm{CO_2}}(I_{\mathrm{CO}} + I_{\mathrm{CO_2}})}\right] \quad (3)$$

where $\Delta m_{\mathrm{total,red}}$ is the wt.% total change in mass from TG data in the temperature transitions 480–680 and 760–1200 °C, M_x is the molecular weight of "x", I_y is the maximum intensity of gas "y" from QMS data in the temperature transitions.

Some assumptions were made to facilitate the calculation of reduction degree: H_2O vaporization and dehydroxylation are the lone causes for weight loss during the temperature transition 40–480 °C, CO_2 generation from the decomposition of carbonates is the lone cause for weight loss during the temperature transition 680–760 °C, CO/CO_2 generation from exclusively iron oxide reduction, and solid carbon gasification leading to iron oxide reduction, is the lone cause for weight loss during the temperature transitions 480–680 and 760–1200 °C.

2.4. Phases and morphology

CBP samples from TG experiments heated to temperatures ranging from 20 to 1250 °C were studied using XRD and SEM. A Siemens D5000 X-ray powder diffractometer using Ni filtered Cu Kα radiation at 40 kV and 50 mA was used for phase analysis of samples. The morphology of different samples was investigated using a Philips XL 30 SEM equipped with energy dispersive spectra (EDS) analysis for chemical mapping.

3. Results and discussion

3.1. TG/DTA/QMS and reduction degree

Fig. 3 shows the TG/DTA/QMS results of heating a CBP sample from 20 to 1200 °C at 10 °C/min in 200 ml Ar/min. Refer to this figure for QMS results when comparing with later figures. The results show agreement with previous work [6,7]. Free moisture is detected from gas analysis in the temperature range of 100–200 °C with ca. 1.6 %wt. loss and a broad endothermic peak in the DTA curve. At temperatures between 300 and 460 °C, chemically bonded water is released with ca. 2.5 %wt. loss accompanied by small endothermic peaks and H_2O generation. Presumably, a decomposition of hydrates has occurred as seen in Fig. 4 illustrating the derivative thermogravimetry (DTG) and derivative differential thermal analysis (DDTA) curves.

Between 450 and 600 °C, CO_2 > CO/evolution is observed with ca. 1.7 %wt. loss. On closer examination shown in Fig. 5, an endothermic peak occurs in the DDTA curve at 500 °C indicating possible carbon gasification at this temperature.

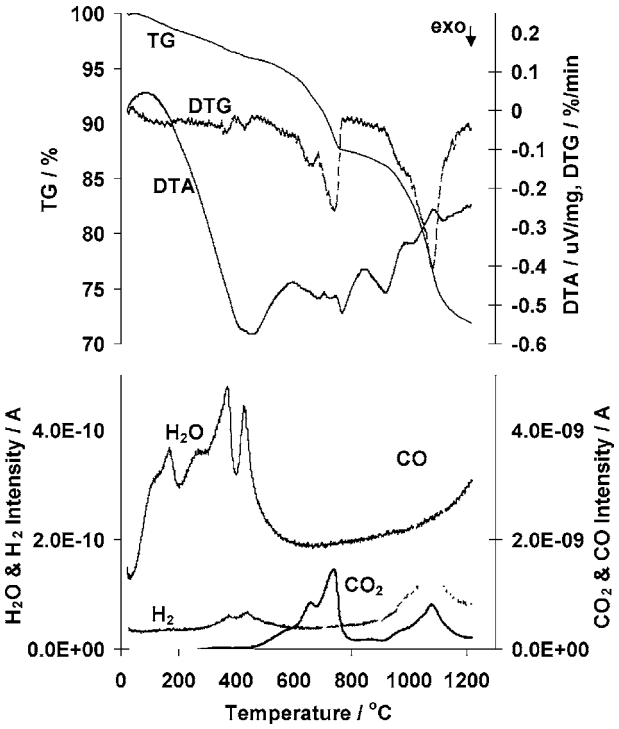

Fig. 3. TG/DTA/QMS results of CBP sample.

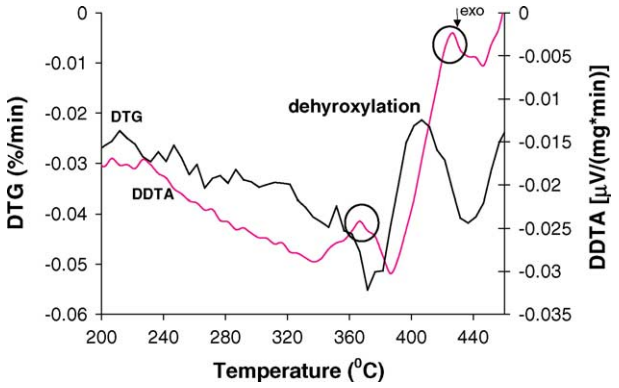

Fig. 4. DTG/DDTA between 200 and 400 °C.

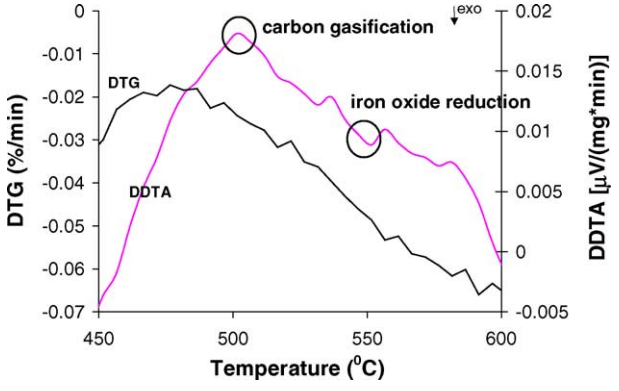

Fig. 5. DTG/DDTA between 450 and 600 °C.

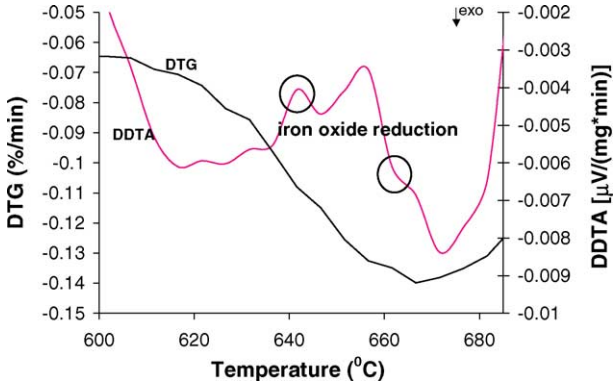

Fig. 6. DTG/DDTA between 600 and 685 °C.

Then an exothermic peak occurs at 550 °C indicating possible iron oxide reduction in this temperature interval.

Next, a new transition occurs in the temperature range of 600–685 °C with ca. 2.3 %wt. loss coinciding with an endothermic peak and an exothermic peak, and $CO_2 \gg CO$ gas evolution. Fig. 6 shows a closer view of this temperature interval highlighting possible iron oxide reduction occurring first as an endothermic reaction at approximately 640 °C and then as a small exothermic reaction at 660 °C.

In the temperature range of 685–800 °C, a transition occurs with two reactions supported by a pair of peaks, endothermic and exothermic, and $CO_2 > CO$ evolution with 4 %wt. loss. The first reaction is possibly a decomposition of carbonates occurring at approximately 700 °C and the second reaction a carbon deposition at 760 °C as shown in Fig. 7.

Above 800 °C, a large transition occurs with ca. 16% total wt. loss in Fig. 3. In the range of roughly 800–900 °C, a small amount of iron oxide reduction can occur coinciding with an endothermic peak at 820 °C and $CO > CO_2$ generation in Fig. 8. Then, some sort of decomposition seems to occur with an endothermic peak at 880 °C and $CO > CO_2$ generation. In the temperature range of 900–1000 °C, further iron oxide reduction can occur corresponding with a large endothermic peak at 950 °C and $CO \gg CO_2$ generation.

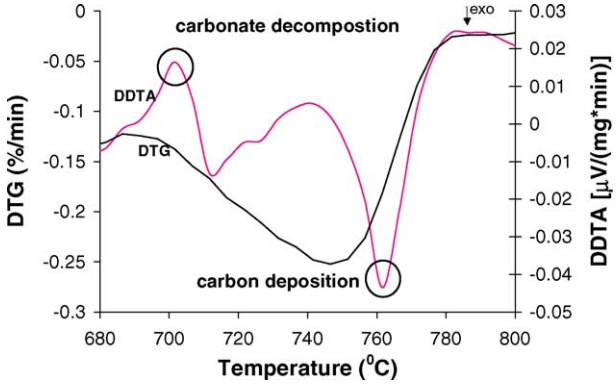

Fig. 7. DTG/DDTA between 680 and 800 °C.

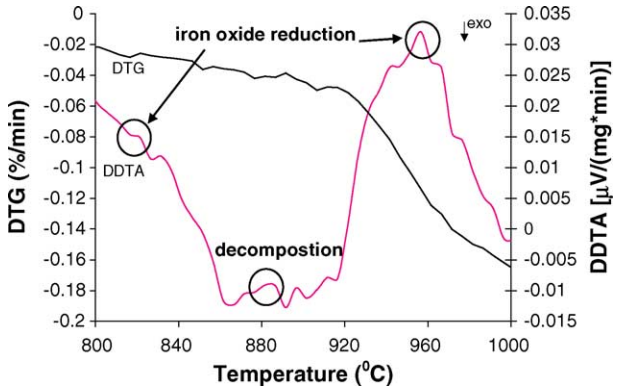

Fig. 8. DTG/DDTA between 800 and 1000 °C.

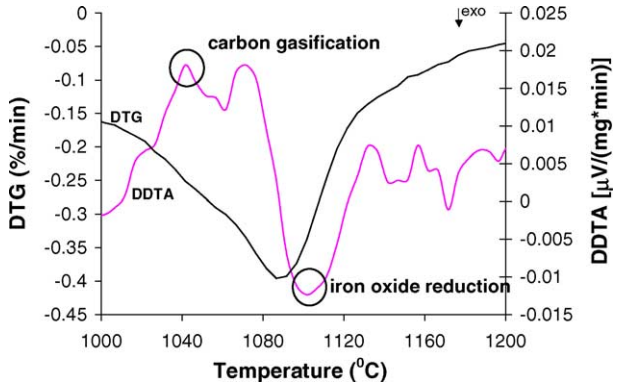

Fig. 9. DTG/DDTA between 1000 and 1200 °C.

Between 1000 and 1200 °C, an endothermic peak occurs at roughly 1040 °C and a subsequent exothermic peak occurs at 1100 °C with $CO \gg CO_2$ generation. These reactions are proposed in Fig. 9 as carbon gasification and iron oxide reduction.

Fig. 10 shows the calculated reduction degree (RD) at different temperatures during thermal analysis of CBP samples. Iron oxide reduction seems to start in a relatively low temperature range, between 500 and 600 °C. A possible explanation is that some carbon gasification, catalyzed by H_2O from dehydroxylation of hydrates, has occurred resulting in

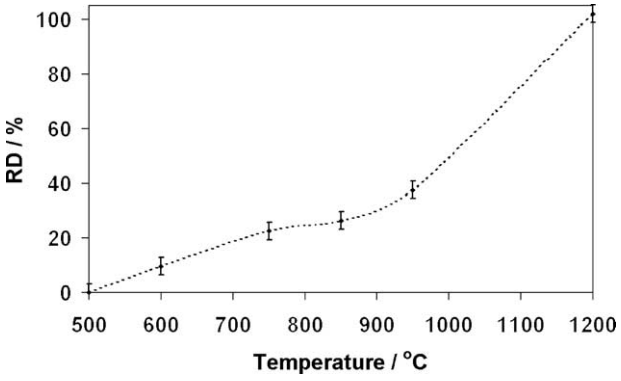

Fig. 10. Calculated reduction degree of CBP sample heated in Ar from 20 to 1200 °C.

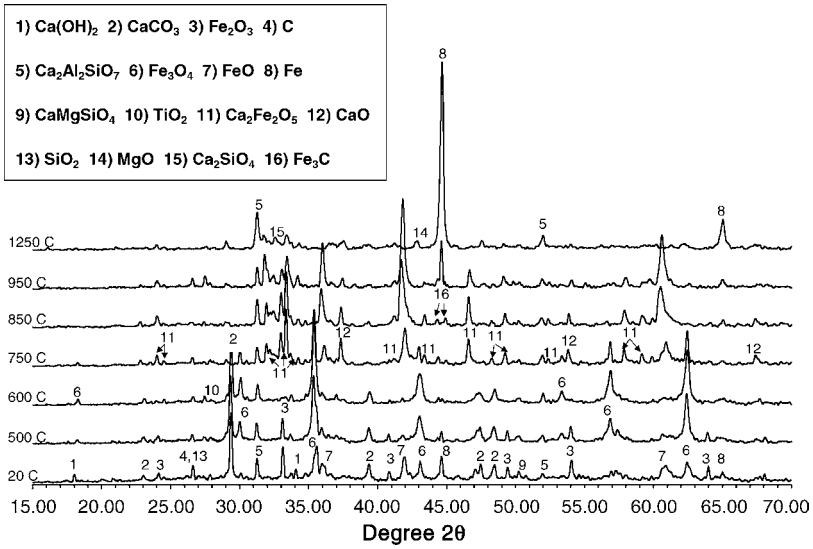

Fig. 11. XRD analysis of CBP samples heated at different temperatures.

local CO generation leading to reduction of Fe_2O_3 to Fe_3O_4 (RD = 9.57%). In the next transition, 600–750 °C, Fe_3O_4 can partly reduce to FeO and then to Fe (RD = 22.45%) coupled with local carbon gasification. During the transition from 750 to 850 °C (RD = 26.29%), reduction of iron oxide is limited possibly due to carbon deposition during this temperature interval. Between 850 and 950 °C, reduction of FeO (RD = 37.52%) could occur with CO_2 generation leading to substantial carbon gasification and a calculated complete reduction of iron oxide (RD = 101.95%) in the range of 950–1250 °C.

3.2. TG and XRD analysis

CBP samples were loaded in to an alumina crucible and heated to various temperatures and then held at these temperatures for 1 h in order to attempt an approach to equilibrium conditions, see Fig. 2. After the 1 h isotherm, furnace effect was stopped and the samples were left to cool in Ar gas until room temperature was reached. Samples heated above 1000 °C were submitted to a controlled cooling at −20 °C/min until 800 °C when furnace effect was completely stopped.

At room temperature, the raw sample contains mostly $CaCO_3$, Fe_3O_4, Fe_2O_3, FeO and Fe, with minor phases of various calcium silicate hydrates, carbon and $Ca(OH)_2$, see Fig. 11. At 500 °C (3.92% total wt. loss), the hydrates in the sample have disappeared. The main reaction occurring below 500 °C is:

$$Me(OH)_2 = MeO + H_2O \quad (4)$$

with Me representing Ca or Mg. At 600 °C (5.87% total wt. loss), peaks of Fe_2O_3 have disappeared supporting a reduction to Fe_3O_4 below this temperature. The reduction is proposed to occur through gaseous intermediates, with CO as the reducing gas, based on noticeable CO_2 generation between 500 and 600 °C in Fig. 3, possibly by the following reactions:

$$H_2O + C = CO + H_2 \quad (5)$$

$$3Fe_2O_3 + CO = 2Fe_3O_4 + CO_2 \quad (6)$$

At 750 °C (10.83% total wt. loss), peaks of Fe_3O_4 and $CaCO_3$ have decreased while peaks of FeO, CaO and $Ca_2Fe_2O_5$ have increased thereby supporting the occurrence of complex carbonate decomposition at 700 °C shown in Fig. 7. The phases detected in XRD also agree with some of the reported phases in Fig. 12 at 700 °C and 65% CO_2/CO mixing ratio. This complex decomposition is most likely comprised of multiple elementary reactions of which the number and order of reactions has not been considered at this time, but a proposed

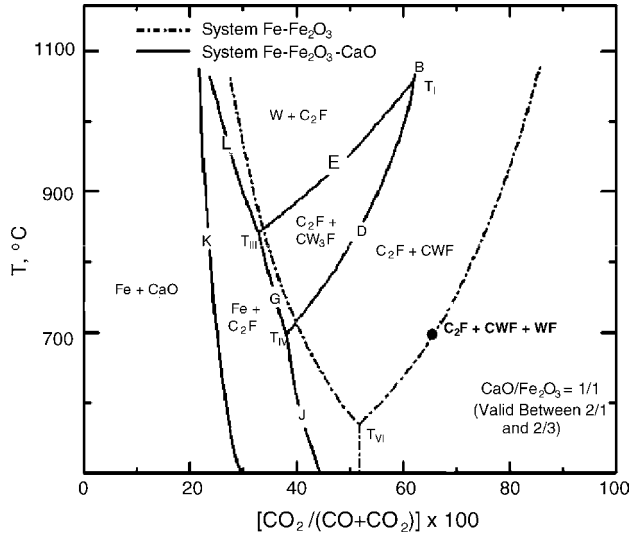

Fig. 12. Fe–Fe_2O_3–CaO system as a function of CO_2/CO mixing ratio; C = CaO, F = Fe_2O_3, W = FeO.

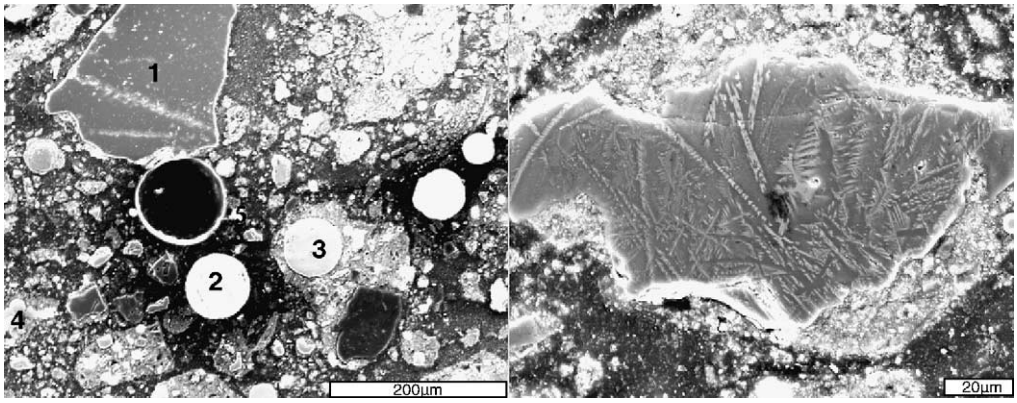

Fig. 13. SEM images of the raw CBPs.

overall reaction is given in Eq. (7). Small peaks of Fe_3C appear at 750 °C as well supporting possible carbon deposition starting at roughly 740 °C. The possible reactions occurring below 750 °C are:

$$Fe_3O_4 + 3CaCO_3 + 2Fe = Ca_2Fe_2O_5 + 3FeO + CaO + 2CO + CO_2 \quad (7)$$

$$3FeO + 5CO = Fe_3C + 4CO_2 \quad (8)$$

At 850 °C (11.70% total wt. loss), the Fe_3O_4 peaks disappear while peaks of FeO and Fe_3C increase. Possibly, the Fe_3O_4 remaining after $Ca_2Fe_2O_5$ formation reduces to FeO, 820 °C in Fig. 8, according to the following reaction:

$$Fe_3O_4 + CO = 3FeO + CO_2 \quad (9)$$

The resulting FeO in turn facilitates further Fe_3C formation via Eq. (8) between 740 and 800 °C.

At 950 °C (14.95% total wt. loss), peaks of CaO, $Ca_2Fe_2O_5$ and Fe_3C have decreased while peaks of FeO and Fe have increased. A partial decomposition of $Ca_2Fe_2O_5$ below 950, 880 °C in Fig. 8, would result in an increase of FeO and Fe in the sample. Furthermore, Fe_3C could reduce some FeO in the sample producing metallic Fe, 950 °C in Fig. 8.

$$Ca_2Fe_2O_5 + 2CO = FeO + Fe + 2CaO + 2CO_2 \quad (10)$$

$$FeO + Fe_3C = 4Fe + CO \quad (11)$$

At 1250 °C (25.87% total wt. loss), the sample contains predominately metallic Fe, Gehlenite ($Ca_2Al_2SiO_7$) and Periclase (MgO) with some other minor calcium silicate phases. A large generation of CO in Fig. 3 between 950 and 1200 °C coupled with the peaks in the DDTA curve in Fig. 9 signifies extensive carbon gasification, Eq. (12), in this temperature interval leading to nearly complete reduction of iron oxide in Eq. (13).

$$C + CO_2 = 2CO \quad (12)$$

$$FeO + CO = Fe + CO_2 \quad (13)$$

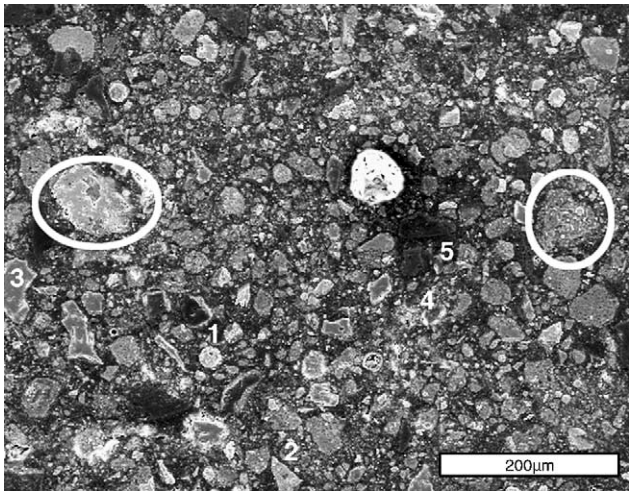

Fig. 14. SEM image of CBP sample heated to 500 °C.

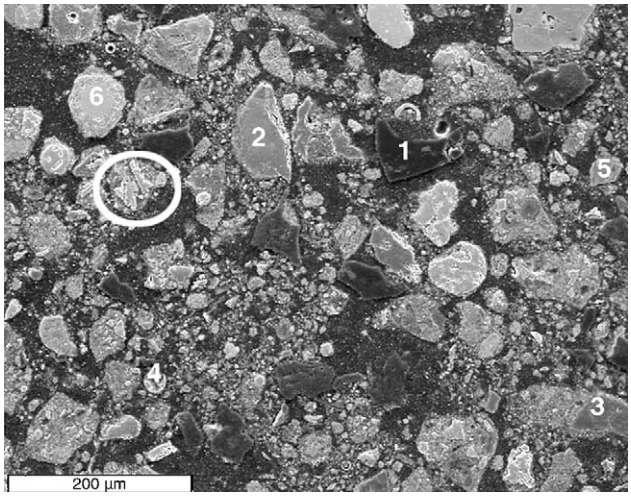

Fig. 15. SEM image of CBP sample heated to 600 °C.

3.3. SEM analysis

Samples from the TG experiments were cast in epoxy resin and polished before observation with SEM. The chemical

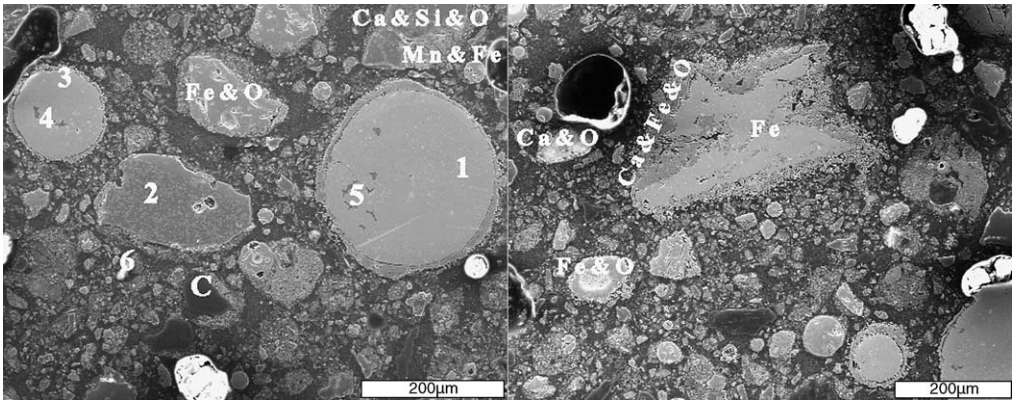

Fig. 16. SEM images of a CBP sample heated to 750 °C.

composition at spots designated by numbers in Figs. 13–16 was investigated using EDS. For a summary of EDS results refer to Table 4. In Fig. 13, the morphological aspect of a raw CBP sample is shown. The micrograph to the left shows an array of discreet particles with various sizes partially enveloped in larger areas of calcium ferrous silicate phases containing some macropores. A typical coke particle is seen below and to the right of spot 3. A separate image of a single particle appears to the right in Fig. 13. This particle has some dendritic structure indicating previous smelting of the metallic phases. The dendrites contain elements Fe > Si and the surrounding areas contain Si > Al > Ca > Fe.

Fig. 14 shows the microstructure of a CBP sample after heating to 500 °C. Here, it is evident that much of the hydrate phase present in the raw material has thermally decomposed. Compared to Fig. 13, particle sizes are much smaller and structural deterioration is observed in some particles (circled in white).

Fig. 15 shows morphological aspects of a CBP sample heated to 600 °C. Evidence of some hematite reduction is present in the form of magnetite lamellae (circled in white) as well as some local oxidation of metallic iron with a dense iron core, spot 6 and a porous iron oxide shell. A general increase in porosity in the sample at 600 °C compared to

Table 4
Summary of EDS image and spot analysis

SEM image	Major elements	Minor elements	Possible phases
Raw CBP (Fig. 13)	Ca, Fe, Si	O, Mg, Al	
Spot 1	Si	O	SiO_2
Spot 2	Si, Mg, O	Ca, Fe	$Ca_x(Fe,Mg)_ySiO_z$
Spot 3	Fe	O	Fe_xO_y
Spot 4	Ca	Fe, O, Si	$Ca_xFe_ySiO_z$
Spot 5	Ca	Fe	Ca_xFe_y
500 °C CBP (Fig. 14)	Fe, Ca	O, Si, Mg, Al	
Spot 1	Fe	O	Fe_xO_y
Spot 2	Fe, Ca	O, Si, Mg, Al	$Ca_x(Mg,Fe,Al)_ySiO_z$
Spot 3	Ca, Si, Mg	O, Al	$Ca_x(Mg,Al)_ySiO_z$
Spot 4	Ca, Si	O, Mg, Al, K, Fe	$Ca_x(Mg,K,Al,Fe)_ySiO_z$
Spot 5	Al, Mg	O	$Mg_xAl_yO_z$
600 °C CBP (Fig. 15)	Ca, Fe	Si, O, Mg, Al	
Spot 1	C	K, Fe, Ca	$(Ca,Fe,K)_xC_y$
Spot 2	Ca, Mg, Fe	Si, Mn, O, Ti	$Ca_x(Mg,Fe,Mn,Ti)_ySiO_z$
Spot 3	Si	K, Al, O	$K_xAl_ySiO_z$
Spot 4	Fe	O, Si	Fe_xSiO_y
Spot 5	Ti, Ca	Fe, Si, Al, O, K	$Ca_x(Fe,Al,Ti,K)_ySiO_z$
Spot 6	Fe	–	Fe
750 °C CBP (Fig. 16), left side	Ca, Fe, Si	O, Al, Mg	
Spot 1	Fe	–	Fe
Spot 2	Ca, Si	Ti, Mn, Fe, O	$Ca_x(Fe,Mn,Ti)_ySiO_z$
Spot 3	Fe	–	Fe
Spot 4	Si, Ca	Mn, K, O, Fe, Ti	$Ca_x(K,Fe,Mn,Ti)_ySiO_z$
Spot 5	Ca, Si	Fe, Ti, Mn, Mg, O	$Ca_x(Mg,Fe,Mn,Ti)_ySiO_z$
Spot 6	Ca, O	≫Fe, Si	CaO
750 °C CBP (Fig. 16), right side, particle shell	Fe, Ca	O	$Ca_xFe_yO_z$

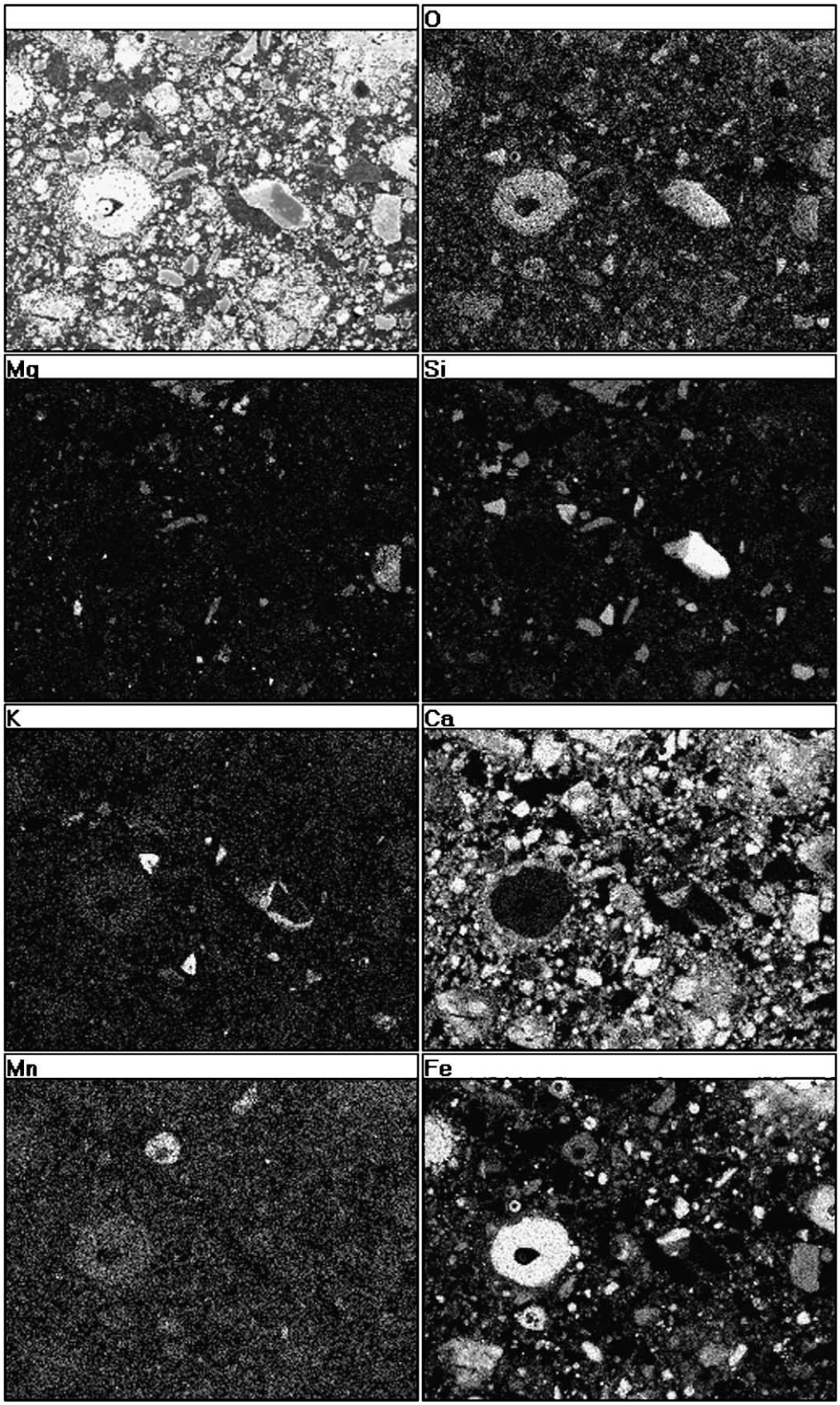

Fig. 17. SEM EDS mapping image from CBP sample heated to 850 °C.

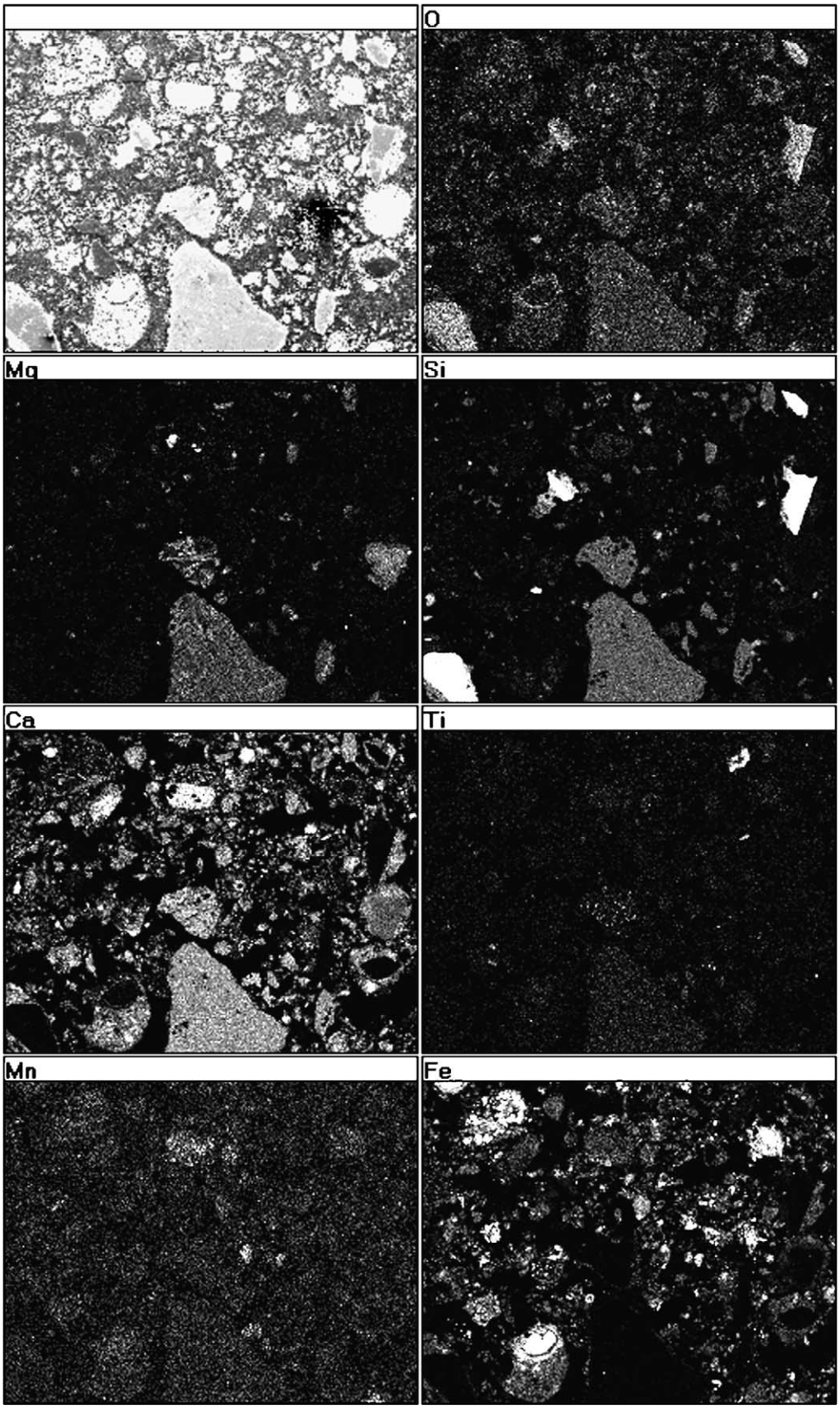

Fig. 18. SEM EDS mapping image from CBP sample heated to 950 °C.

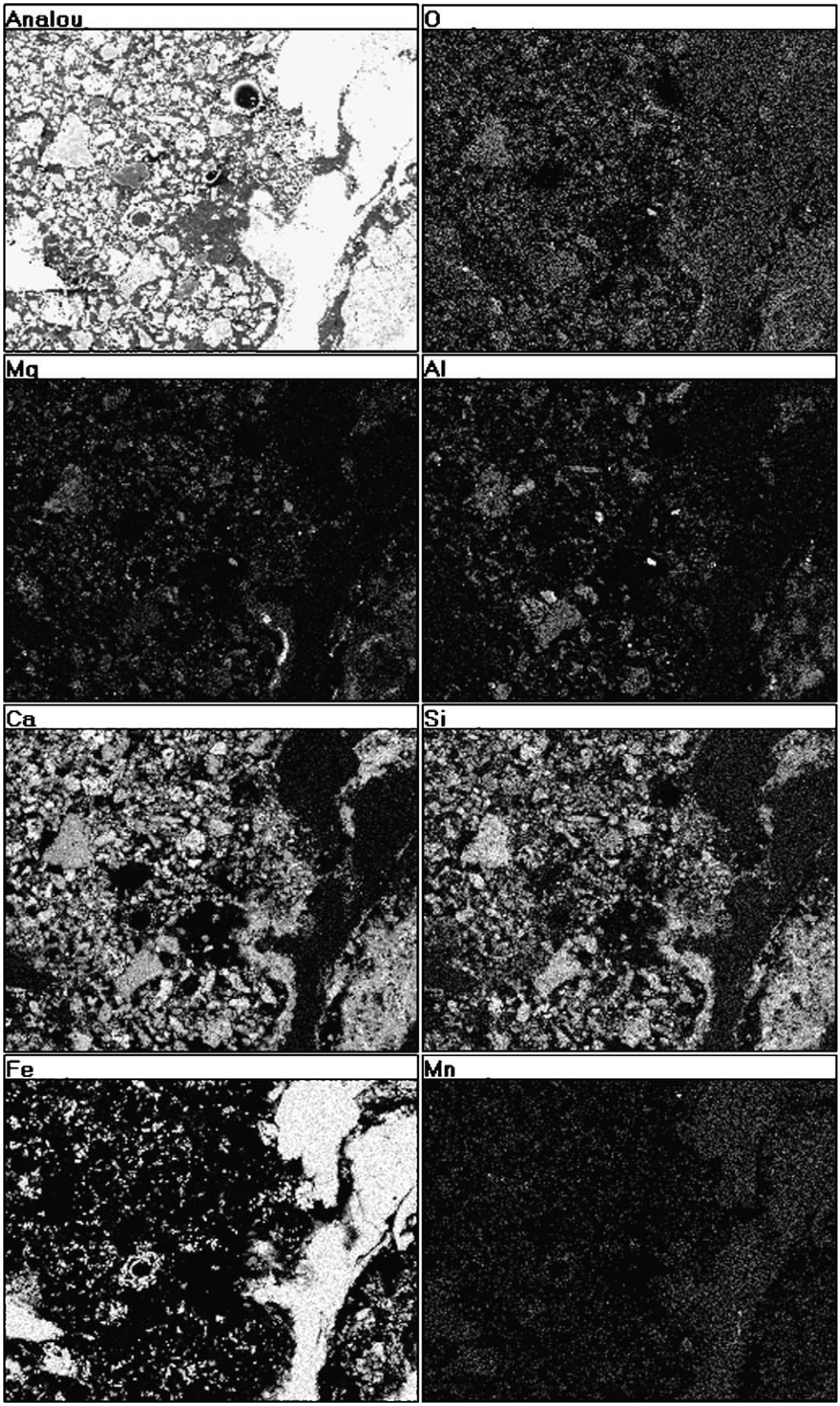

Fig. 19. SEM EDS mapping image from CBP sample heated to 1200 °C.

500 °C indicates possible local gas evolution around some individual particles.

Fig. 16 contains two micrographs from a sample heated to 750 °C. The images show that significant change has occurred in the sample between 600 and 750 °C. In the left image, a calcium ferrous oxide phase has accumulated as a shell around large metallic iron particles, spots 1 and 3, with inclusions, spots 4 and 5. Smaller particles of iron oxide, coke and slag (spot 2) lie in the vicinity of the larger metallic iron particles and even some traces of CaO shown in spot 6. The image to the right supports the proposed complex carbonate decomposition in Eq. (7).

Fig. 17 shows EDS mapping of a sample after heat treatment to 850 °C. The micrograph in the upper left corner of the figure shows the analog image of the entire sample while the remaining micrographs show the dispersion of various elements in the sample. Elements Fe, Ca and O dominate the image with minor amounts of Si, Mg, Al, K and Mn. The majority of Fe content overlaps with Ca content in the sample except for smaller metallic Fe particles and some larger porous iron oxide particles. Si, K and Al content overlap with each other while Mg overlaps with Ca and Mn with Fe.

Fig. 18 shows the EDS mapping results from a sample heated to 950 °C. Areas containing Fe in the sample show large amounts of disintegration except for small amounts of dense metallic iron formation. This could possibly be explained by large $Ca_2Fe_2O_5$ particle's dissolution to smaller CaO, FeO and Fe_{met} particles in Eq. (10) coinciding with extensive gas evolution in Eqs. (11) and (12). Silicon oxide content is large in certain particles, possibly as a remnant from carbon gasification of coke and coal particles. Calcium dominates the sample combining with other elements forming a slag matrix.

At 1200 °C, the morphology of the CBP sample is dominated by metallic iron formation surrounded by calcium silicate slag with minor inclusions of Al, Mg, Mn and V. Fig. 19 illustrates these SEM results.

4. Conclusions

These conclusions can be drawn from the current work:

- With the given conditions, heat treatment of the CBP sample from 20 to 1200 °C at 10 °C/min in 200 ml Ar/min, 100% calculated reduction degree of contained iron oxides is possible.
- Hydrates and carbonates in the CBP sample play a significant role in the reduction characteristics of iron oxides.
- Fe_2O_3 is reduced to Fe_3O_4 between 500 and 600 °C.
- Carbonate decomposition occurs as part of a complex series of reactions initiating at ∼700 °C under given conditions forming $Ca_2Fe_2O_5$ among other products.
- Fe_3O_4 is reduced to FeO and between 640 and 850 °C.
- FeO is reduced to Fe between 850 and 1200 °C.

Acknowledgements

I wish to thank my colleagues at the Division of Process Metallurgy, especially Dr. Nourreddine Menad, for suggestions and assistance during the course of this work and financial support from VINNOVA is also gratefully acknowledged.

References

[1] A. Fleischanderl, et al., Aspect of recycling of steelworks by-products through the BOF, SEAISI Q. 28 (April (2)) (1999) 51–60.
[2] R.L. Nyirenda, The processing of steelmaking flue dust: a review, in: Proceedings of the First International Conference—Minerals Engineering '91, Singapore, 1991, pp. 1003–1025.
[3] T. de Bruin, L. Sundqvist, Briquetting—one way of treating by-products at SSAB Tunnplåt in Luleå, in: ICSTI/Ironmaking Conf. Proc., Toronto, Canada, 1998, pp. 1263–1273.
[4] M.C. Mantovani, C. Takano, The strength and high temperature behaviours of self-reducing pellets containing EAF dust, ISIJ Int. 40 (3) (2000) 224–230.
[5] J.A.C. Lopez, et al., Development of B.F. Flue Dust Briquette for Recycling in BOF at AHMSA, ICSTI, Toronto, Canada, 1998, pp. 1275–1279.
[6] G.-s. Liu, et al., Thermal investigations of direct iron ore reduction with coal, Thermochim. Acta 410 (2004) 133–140.
[7] R.T. Wargo, et al., Evaluation of cold-bonded revert briquettes at the USS Gary No. 8 blast furnace, in: Ironmaking Conf. Proc., vol. 50, Washington, DC, 1991, pp. 69–87.